NANO LETTERS

2008
Vol. 8, No. 7
2035-2040

Fabrication of a Well-Ordered Nanohole Array Stable at Room Temperature

K. Aït-Mansour,*,† A. Buchsbaum,‡ P. Ruffieux,† M. Schmid,‡ P. Gröning,† P. Varga,‡ R. Fasel,† and O. Gröning*,†

Empa, Swiss Federal Laboratories for Materials Testing and Research, Feuerwerkerstrasse 39, 3602 Thun, Switzerland, and Institut für Allgemeine Physik, Technische Universität Wien, Wiedner Hauptstrasse 8-10/134, 1040 Wien, Austria

Received May 9, 2008

ABSTRACT

We report on the fabrication of a new type of nanotemplate surface consisting of a hexagonally well-ordered array of one monolayer deep holes with a tunable size of about 4 nm² and a fixed spacing of 7 nm. The nanohole array fabrication is based on the strain-relief trigonal network formed in the 2 monolayer Ag on Pt(111) system. Removing about 0.1 ML of the Ag top layer of this surface structure, for example, by He- or Ar-ion sputtering, leads to the formation of nanoholes at specific domains of the trigonal network, which are stable at room temperature.

Nanometer scale periodic structures at single crystal surfaces are highly interesting, not only from a fundamental point of view but also for technological applications: They can be used as templates to organize adsorbed atomic and molecular species into nanostructures responding to desired features at dimensions which are not accessible with lithographic techniques.[1] In this context, vicinal surfaces of Au(111) have been intensively used in recent years as templates to grow nanostructures because of the well-known higher selective adsorption at step edges with respect to the narrow, bare terraces, where adsorption is also found to vary from region to region depending on the Au top-layer atomic stacking.[2–5] Atomic and molecular nanostructures grown on these vicinal surfaces and replicating exactly the surface periodicity have been successfully fabricated.[2–4] In addition, the misfit dislocation structures that are spontaneously formed on numerous hexagonal surfaces of thin films in metal heteroepitaxial systems (Ag/Pt,[6] Ag/Ru,[7,8] Au/Ni,[9] Ag/Cu,[10] etc), in order to relieve the strain induced by the lattice mismatch between the substrate and the overlayer, as well as the natural herringbone reconstruction of the clean Au(111) surface[11] are good template candidates to control the nucleation and growth of nanostructures.[12–16] For instance, the triangular structure of two monolayers (ML) of Ag on Pt(111), the so-called "trigonal network" according to its first observation,[6] associated with ordered misfit dislocations has been found to be very efficient in the self-organized growth of small metal islands[12] as well as in the site-selective adsorption and self-assembly of organic molecules.[13,14]

In this communication, we report an unprecedented template surface which appears ideal for templating the growth of well-ordered nanostructures in the sub-10 nm range. The template consists of a remarkably regular hexagonal superlattice of triangular holes (vacancy islands) of adjustable size and 1 ML Ag depth formed on the 2 ML Ag/Pt(111) trigonal network. The nanoholes are created at room temperature (RT) by He- or Ar-ion sputtering of the 2 ML Ag/Pt(111) dislocation network surface. Recently, studies have reported nanoholes, however filled with sulfur, which also self-organize in a hexagonal lattice, on another system which is 1 ML Ag/Ru(0001).[17] For this system, the surface is exposed to a submonolayer coverage of S, which substitutes part of the Ag film in order to strongly and directly bind to the Ru substrate.[17] In contrast to this case, where the stability of the nanoholes is simply due to the filling with S, the nanoholes presented in our work are voids (i.e., free of any other adsorbate) and stabilized by intrinsic periodic reconstructions of the 2 ML Ag/Pt(111) trigonal network which are buried in the deeper layers. Furthermore, whereas on the 2 ML Ag/Pt(111) dislocation network surface cooling down the sample to 110 K is needed to kinetically control the self-organized growth of nanostructures,[12] the nanohole pattern presented here can be used to assemble well-ordered nanostructures even at RT, as we demonstrate here with C_{60} chosen as a test molecule.

Our experiments were carried out in three different multichamber ultrahigh vacuum systems with base pressures of a few 10^{-10} and 10^{-11} mbar in the preparation and scanning tunneling microscopy (STM) chambers, respec-

* Corresponding authors. E-mail: (K. A.) Kamel.Ait-Mansour@empa.ch; (O. G.) Oliver.Groening@empa.ch.
† Swiss Federal Laboratories for Materials Testing and Research.
‡ Technische Universität Wien.

10.1021/nl8013378 CCC: $40.75
Published on Web 06/12/2008

tively. The STM measurements presented here were obtained with three different instruments (commercially available from Omicron): A low-temperature (LT) STM[13] operated at 77 K (STM images shown in Figure 1), an RT micro-STM[18] (Figures 2–4) and a variable-temperature STM[4,5] operated at RT (Figure 5). Mechanically cut Pt/Ir and electrochemically etched W STM tips were used. The STM images were recorded in the constant-current mode, the stated voltage refers to the electric potential of the sample with respect to the tip. The STM images have been processed with the WSxM software.[19] The Pt(111) single-crystal substrate was cleaned by several cycles of Ar-ion sputtering (1−2 keV) at RT and then at 850 °C, resulting in large terraces (with widths reaching more than 200 nm), separated by monoatomic steps, free of impurities, as checked by X-ray and ultraviolet photoelectron spectroscopy. Ag (purity = 99.99%) was evaporated (below 1×10^{-9} mbar) from either a home-built evaporator or an Omicron metal evaporator, both using electron-bombardment heating, with a rate of about 0.4 ML per minute as monitored by quartz microbalance and verified by STM. One ML Ag refers to the completion of a closed atomic layer on Pt(111), as calibrated by STM. The 2 ML Ag film was deposited with the substrate held at RT and subsequently annealed to 800 K (during 5 min), as reported elsewhere.[6,12,13] The nanoholes on the 2 ML Ag/Pt(111) trigonal network surface were created either by He- or Ar-ion sputtering at RT and, in both cases, the incidence of the ion beam was 45° off the sample surface normal. He- and Ar-ion sputtering were done at accelerating voltages of 1 kV and 400 V, respectively. The sputter time to achieve the removal of similar amounts of silver was about 100 times longer for He as compared with Ar.

The pristine 2 ML Ag/Pt(111) dislocation trigonal network prepared as outlined above is shown in the STM image of Figure 1a. The fast Fourier transform (FFT) of the STM image (inset in Figure 1a), with first- and second-order spots, shows the very regular character of the trigonal network. With an average period of about 7 nm, the trigonal network can be regarded as a (25 × 25) superstructure with respect to the underlying Pt(111) atomic lattice. According to the first report of this trigonal network and the proposed structural model,[6] the first Ag layer is expected to be pseudomorphic with the Pt(111) substrate, whereas the second (topmost) Ag layer relaxes the 4.3% Ag−Pt lattice mismatch induced strain by forming Shockley partial dislocations, associated with the crossing dark lines (corresponding to topographic depressions) in the STM image of Figure 1a which are aligned along the Ag⟨1−10⟩ (and Pt⟨1−10⟩) close-packed directions. As can be seen in Figure 1a, the dark lines separate three types of domains present in the superstructure unit cell: A hexagonal domain where the Ag atoms are expected to be in face-centered cubic (fcc) stacking and two differently sized triangular domains where the Ag atoms are expected to be in hexagonally close-packed (hcp) stacking.[6] This proposed atomic stacking was intuitively inspired by the one of the herringbone reconstruction of Au(111), but, so far, it has never been elucidated in detail. In analogy to this originally proposed top-layer atomic

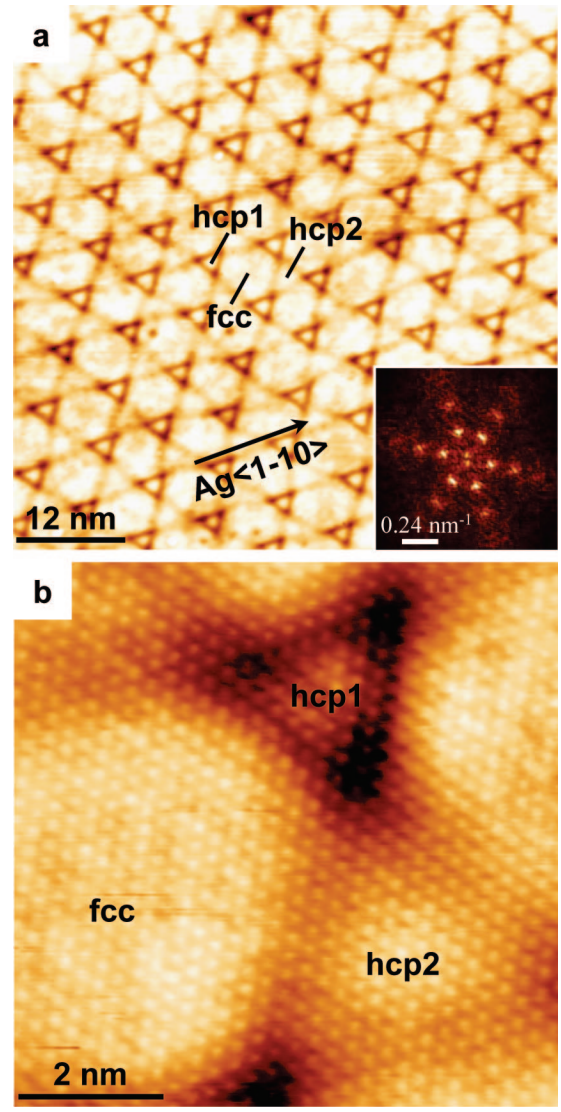

Figure 1. Two ML Ag/Pt(111) trigonal network. (a) Topographic LT-STM image 60 nm × 60 nm (−2 V, 1 nA) where three types of domains (fcc, hcp1, and hcp2, see text) can be observed, which are separated by dark lines appearing lower than the rest of the surface (maximum depression ~0.4 Å at the hcp1 corners). Inset, FFT of the STM image showing the high degree of order of the trigonal network. (b) Atomically resolved LT-STM 7.5 nm × 7.5 nm (−40 mV, 40 nA) showing that the topmost Ag layer is free of cut partial dislocations between the three types of domains, unlike what was anticipated in the model originally proposed in ref 6.

stacking structure, we call "fcc" the hexagonal domain and "hcp1" and "hcp2" the small and big triangular domains, respectively (Figure 1a). It should be noted that the lines surrounding the hcp1 domains appear markedly deeper than the rest of the trigonal network surface, in particular the hcp1 corners where the maximum depression of about 0.4 Å occurs.

Figure 2a shows the surface morphology after performing a cycle of He-ion sputtering of 45 min. As can be seen, the sputtering procedure gives rise to a well-ordered superlattice of holes located exactly at the hcp1 regions of the trigonal network and having preferentially a triangular shape, as shown in the close-up observation of the central area of Figure 2a which is displayed in Figure 3a. The height profile

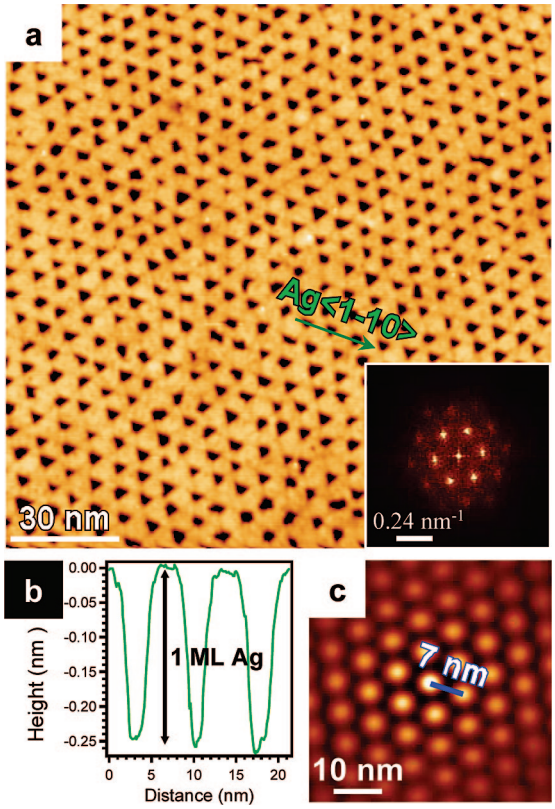

Figure 2. The well-ordered nanohole pattern produced by He-sputtering of the 2 ML Ag/Pt(111) trigonal network. (a) Overview RT-STM image 150 nm × 150 nm (−1 V, 0.1 nA) where the hcp1 regions of the 2 ML Ag/Pt(111) trigonal network are removed, giving rise to a regular superlattice of nanoholes, as shown by FFT (inset). (b) Height profile along the Ag⟨1−10⟩ direction indicated in (a) showing that holes are 1 ML Ag(111) deep. (c) Self-correlation image of (a) demonstrating that the nanohole pattern replicates exactly the periodicity (7 nm) and symmetry of the trigonal network structure.

of Figure 2b, measured along the Ag⟨1−10⟩ direction indicated in Figure 2a, shows that the depth of the holes is about 2.5 Å, which corresponds well to the height of a monoatomic step of Ag(111) (2.4 Å). The FFT image inset in Figure 2a shows that the hole pattern replicates exactly the symmetry and periodicity of the 2 ML Ag/Pt(111) trigonal network, which is also confirmed by the self-correlation image displayed in Figure 2c. The distribution of the hole area displayed in the histogram of Figure 3b was obtained from the analysis of the STM image of Figure 2a. Figure 3b shows that the sizes of the holes follow a Gaussian distribution with a peak situated at about 6.9 nm^2. The area of a hole has been estimated with the assumption that the real atomic step is 3 Å away from the position where the STM detects the half-height of the step.[4] The corresponding amount of sputtered Ag is about 0.16 ML. The average size found here for the holes is larger than the area of the hcp1 domains which is about 3.6 nm^2 (as the hcp1 triangle is roughly equilateral with an edge of about 2.9 nm) and corresponds to about 0.09 ML Ag. The difference between the average area of the created holes and the average hcp1 area shows that Ag atoms surrounding the hcp1 regions are removed together with the hcp1 regions themselves after He sputtering, which can also be seen by comparing the STM images of Figures 1a and 3a. It is possible to reduce the size of the created holes, for instance, by reducing the He-sputtering time. As can be seen in Figure 3c, where the He-sputtering time has been halved compared with the situation depicted in Figure 3a, the average hole size is now decreased to about 2.8 nm^2 (Figure 3d), which is lower than the average area of the hcp1 regions (3.6 nm^2). The control of the nanohole size demonstrated here is of major importance, as this can be used to control the size of many postadsorbed nanostructures.

A remarkable property of the nanohole pattern is its high stability at RT. Even 24 hours after the fabrication, no significant structural changes can be observed. It is clear that such a pattern on an unreconstructed metal surface is energetically highly unfavorable, because of the considerable number of atoms, at the steps that constitute the boundaries of the holes, which have a reduced coordination. The stability of the pattern is even more surprising in view that on Ag(111) small vacancy islands are not stable at RT because of the high mobility of the Ag surface atoms resulting from a rather flat surface potential landscape and leading to the rapid disappearance of the vacancy islands (in a few minutes).[20] It is therefore evident that the formation and stabilization of this regular nanohole pattern can occur only in the presence of periodic reconstructions buried in the deeper layers of the 2 ML Ag/Pt(111) trigonal network, in particular in the Pt(111) substrate.

In agreement with this, the atomically resolved STM image of the trigonal network displayed in Figure 1b shows that the atomic structure of the topmost layer is close to hexagonal and free of partial dislocations, in contrast to the originally proposed model[6] suggesting that the sole reconstructions in the trigonal network structure occur in the Ag top layer in form of partial dislocations. In this context, it is worth mentioning that a trigonal network very similar to the one of 2 ML Ag/Pt(111) has recently been reported elsewhere on a film of 2 ML AgAu alloy on Ru(0001), where the topmost layer was also found to be free of any partial dislocations.[8] Thus, supported by embedded-atom method calculations, which nevertheless were performed on the 2 ML Ag/Pt(111) system ("to avoid the complex issues associated with an alloy"), the authors of this study (ref 8) proposed that the Shockley partial dislocations take place in the first (underlying) layer of the 2 ML film in both systems AgAu/Ru(0001) and Ag/Pt(111). We believe that partial dislocations occurring in the first layer of the 2 ML Ag/Pt(111) trigonal network can not explain alone the RT formation and stability of the ordered nanoholes. One needs to conclude that the dislocations go deeper; that is, they extend into the Pt substrate, which then goes beyond the model proposed in ref 8. Let us note that bimetallic systems exist, where partial dislocations occur in the substrate and not in the overlayer. For instance, in the case of Cr/Pt(111), an ordered hexagonal superstructure has been interpreted as dislocation lines in the top layer of Pt(111).[21] In addition, in the case of 1 ML Au/Ni(111)[9] and 1 ML Ag/Cu(111),[10] dislocation loops occur in the topmost layer of the substrate

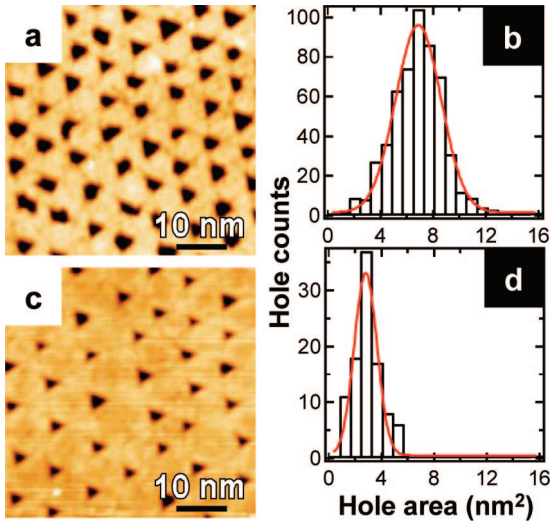

Figure 3. Control of the average size of the nanoholes created on 2 ML Ag/Pt(111). (a) Close-up RT-STM image 50 nm × 50 nm (−1 V, 0.3 nA) measured in the central region of Figure 2a. (b) Analysis of the nanoholes from the STM image of Figure 2a showing that the holes have an average size of 6.9 nm^2 (peak of the Gaussian distribution). (c) RT-STM image 50 nm × 50 nm (−1 V, 0.1 nA) of another prepared nanohole pattern where the He-sputtered time has been roughly halved compared with the situation of (a). (d) Analysis of nanoholes from an STM image of 90 nm × 90 nm containing the region shown in (c) showing that the holes have now an average size reduced to about 2.8 nm^2.

(Ni(111) or Cu(111)), which gives rise to triangular structures observable through the 1 ML film (Au or Ag, respectively). Finally, a recent work on a semiconductor system of 5 ML InAs/GaAs has reported a trigonal network, very similar to the one of 2 ML Ag/Pt(111), where the misfit dislocations are expected to be buried at the InAs/GaAs interface.[22] It is known that the trigonal network of 2 ML Ag/Pt(111) as well as the other triangular structures in metallic systems mentioned above are stable reconstructions resulting from irreversible transitions which can be thermally activated by annealing metastable structures.[6,8–10] But what is remarkable here is that, once the trigonal network of 2 ML Ag/Pt(111) is formed, its fingerprint is still observed even after sputtering away the hcp1 regions, which is only possible with significant reconstructions in Pt(111).

The principal question that we want to address now concerns the formation mechanism of the nanoholes. During sputtering, the He ions hit the surface homogeneously, and there is no valid reason why the top-layer Ag atoms of only the hcp1 regions would be removed whereas the other (fcc and hcp2) regions would be completely indifferent vis-à-vis to He sputtering. Indeed, the 1 kV accelerating voltage of the He ions is far too high to "see" any small difference in binding energy between the top-layer Ag atoms of the distinct regions of the trigonal network, which eventually could be related to a difference in the atomic stacking. Density-functional theory calculations showed that the difference between fcc and hcp sites is less than 10 meV for an Ag adatom on 1 ML Ag/Pt(111),[23] which needs to be compared with the total binding energy of the order of 2 eV. Therefore, the hole pattern seen in Figure 2a can only be understood as an equilibrium ground state to which the system evolves after atomic diffusion processes occurring at the surface. Two principal processes lead to the occurrence of the nanohole pattern: (i) first, homogeneous creation of atomic vacancies at the surface in all three regions (fcc, hcp1, and hcp2), and (ii) second, fast self-organization of the vacancies on the surface in form of diffusion from the fcc and hcp2 regions to the hcp1 regions (i.e., diffusion of the residual atoms in the hcp1 regions into the fcc and hcp2 regions).

The question why the vacancies aggregate only in the hcp1 regions still needs to be answered. It should be noted that these regions are the smallest on the trigonal network surface. In the case of the herringbone reconstruction of Au(111), which shows fcc and hcp stacking domains for the topmost layer, the difference in the widths of the two domains reflects a difference in energy of stacking, and the narrower hcp domains are less favorable than the wider fcc domains which represent the bulk stacking (see ref 11 and references therein). In analogy, an interpretation of the hcp1 region as energetically least favorable stacking domain among the three types of domains can be undertaken. This might explain why the hcp1 regions are those where the vacancy islands are formed and therefore also why these small vacancy islands do not destroy the periodic buried reconstructions on which the trigonal network is built up. It should be interesting to perform sputtering experiments on two other elsewhere reported trigonal networks very similar to the one of 2 ML Ag/Pt(111) which are the 2 ML AgAu/Ru(0001)[8] and the 5 ML InAs/GaAs(111).[22] Compared with 2 ML Ag/Pt(111), the atomic mobility at RT might be similar on 2 ML AgAu/Ru(0001) but lower on 5 ML InAs/GaAs(111).

The nanoholes discussed above can also be created locally by moving atoms of the topmost layer with the STM tip at RT, as shown in Figure 4. By lowering the tunneling resistance and thus increasing the interaction between the tip and the surface atoms, the tip snatches Ag atoms from the scanned regions and therefore modifies locally the surface. The missing Ag atoms in the triangular holes at the hcp1 regions in Figure 4b have most probably diffused to step edges which are favorable sites for their adsorption, a process which can easily occur at RT. As can be seen in Figure 4b, the fcc and hcp2 regions, close to the cleared hcp1 regions, which were also scanned with the low tunneling resistance, are still intact after this STM tip experiment. So this result is the local analogue to what we obtained by He-ion sputtering in Figures 2a and 3a,c. However, the STM tip induced formation mechanism of the holes may be different compared with the one by He-ion sputtering. Tip-induced displacement of surface atoms is only possible if forces (attractive or repulsive) exerted by the STM tip are sufficiently large in order to move atoms out of their equilibrium position. For a nanostructured surface with laterally inhomogeneous properties, one can expect that this can be used to selectively remove atoms in regions where the surface atoms have the lowest binding energy, although the energy difference might be of the order of a few tens of millielectronvolts.[23] This explanation is supported by the observation of instabilities only on the hcp1 regions when

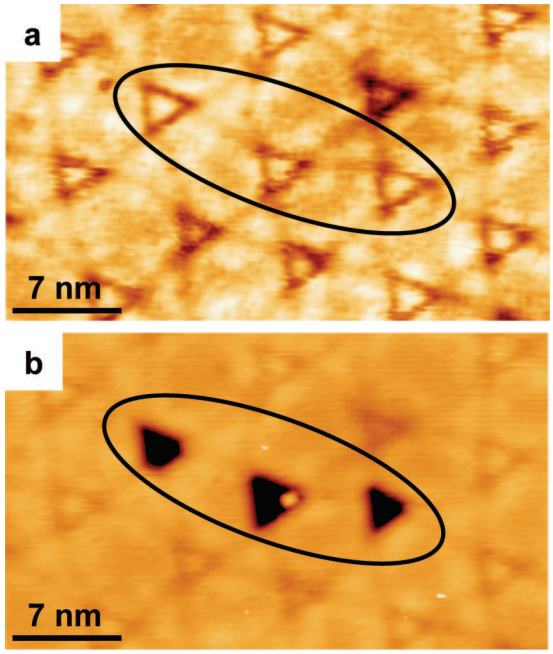

Figure 4. Creation of triangular holes at the hcp1 regions of the 2 ML Ag/Pt(111) trigonal network with the STM tip at RT. (a,b) RT-STM images 35 nm × 19 nm of the same surface region on 2 ML Ag/Pt(111). After measuring (a) (−1 V, 0.1 nA), the scanning window was reduced into a smaller surface area containing the region shown by an ellipse and in (a), which was scanned with a very low tunneling resistance (77 kΩ: −1 mV, 13 nA), after that the image (b) (−0.6 V, 0.1 nA) was recorded.

scanning with usual tunneling parameters at RT (Figure 4a). These instabilities indicate that the surface atoms of the hcp1 regions can be more easily displaced from their equilibrium position, although here the interaction with the tip is not yet sufficient to remove the atoms from the layer. We believe that the formation of the triangular holes in Figure 4b results from preferential removal of only hcp1 region Ag atoms with the STM tip, because of the fact that the binding energy of the Ag atoms in these smaller regions is lower with respect to the other bigger (hcp2 and fcc) regions. At this stage, an unspecific atom removal by the tip and a subsequent vacancy diffusion as for the He sputtering can not be completely excluded. However, the instabilities in the STM topography observed only in the hcp1 regions suggest otherwise.

To show the potential of the well-ordered nanohole as a template to grow ordered nanostructures, we evaporated a thin film (of about 0.1 ML) of C_{60} at RT (see Figure 5). The nanohole pattern prior to C_{60} was prepared by Ar sputtering (as indicated above) for which the sputtered amount of Ag was in between those shown in Figure 3a,c. On standard noble metal surfaces like Ag(111) and Au(111), it is well-known that the C_{60} molecule is highly mobile at RT and initially adsorbs (except for pinning at defects on bare terraces) exclusively at step edges, which are the sole sites of nucleation of C_{60} islands.[4,24] We also found that the C_{60} molecule at RT is still mobile on the 2 ML Ag/Pt(111) dislocation trigonal network and is able to cross the dislocation lines.[13] Here, on the nanohole pattern, the C_{60} molecules are trapped in the holes and grow in ordered nanoclusters which are composed of 1 to 10 molecules (Figure 5b) and

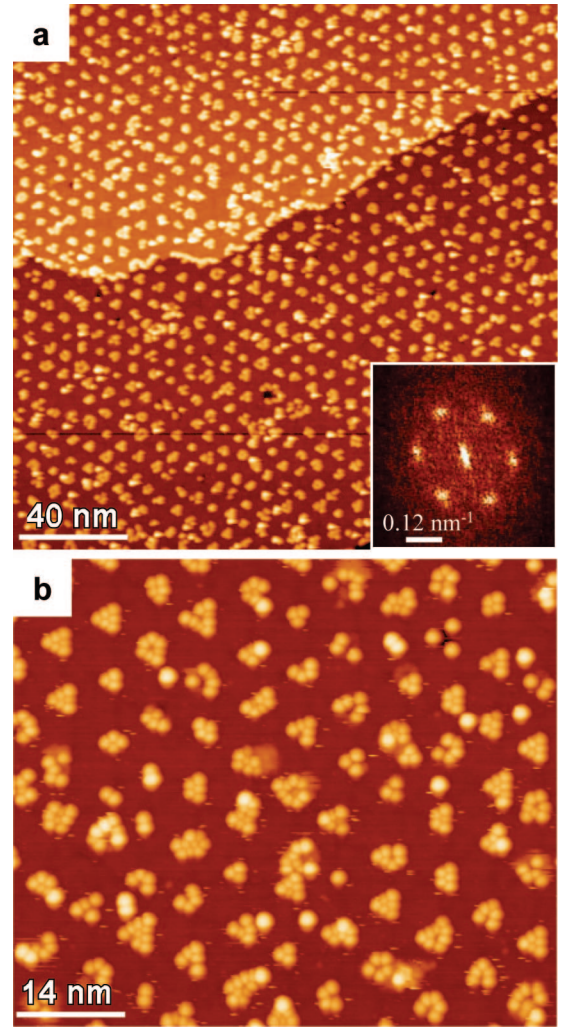

Figure 5. Example of potential application of the well-ordered nanohole pattern: self-organized growth of C_{60} nanoclusters at RT. (a) Overview RT-STM image 200 nm × 200 nm (−2 V, 50 pA) showing long-range order of a molecular nanostructure array replicating the hexagonal symmetry of the nanohole pattern, which is also illustrated by FFT (inset). (b) Close-up RT-STM image 70 nm × 60 nm (−2 V, 50 pA) of the array of C_{60} nanoclusters trapped inside the nanoholes.

replicate exactly the periodicity and hexagonal symmetry of the nanohole array, which is clearly visible in Figure 5a and confirmed by the corresponding FFT (inset in Figure 5a). Note that the C_{60} nanocluster growth in the holes takes place despite the fact that step edges terminating the bare terraces are not completely occupied by C_{60} molecules (Figure 5a). In addition to the molecular clusters decorating the holes, some C_{60} molecules (appearing brighter in Figure 5b) are adsorbed on 2 ML of Ag (probably because of the pinning at defects induced by the sputtering procedure) and then appear higher by roughly 1 ML of Ag, which confirms that the former are unambiguously adsorbed inside the holes. The fact that the holes trap the C_{60} molecules is not surprising because the hole boundaries are nothing else than step edges which are well-known to be energetically more favorable adsorption sites for molecules[4,5,24,25] as well as metallic nanostructures.[2,3] We expect that the nanocluster self-organized growth on the well-ordered nanohole pattern

demonstrated here for C_{60} can be extended to many other molecules as well as metals, in particular those which might have interesting electronic or magnetic properties to study.

In conclusion, we reported in this communication on the fabrication of a well-ordered superlattice of clean nanoholes by He- or Ar-ion sputtering the topmost layer of the 2 ML Ag/Pt(111) dislocation trigonal network at RT. The holes have a depth of exactly 1 ML Ag, and their average size can be varied by the amount of sputtered Ag. The formation of the regular nanohole pattern and its exceptional stability at RT are due to the presence of periodic reconstructions buried in the deeper layers of the 2 ML Ag/Pt(111) trigonal network, in particular in the Pt(111) substrate. Completely ignored in the previous works on this system, these buried Pt reconstructions are those on which the trigonal network structure is built up. We used C_{60} molecules to probe the site-specific RT adsorption on the nanohole pattern and successfully fabricated regularly distributed C_{60} nanoclusters trapped in the holes which therefore replicate the periodicity and hexagonal symmetry of the nanohole template surface. This C_{60} nanocluster self-organized growth shows that the nanohole pattern has a great potential of applications in the RT growth of many other well-ordered molecular and atomic nanostructures of very small size, eventually desired for studying their physical (electronic, magnetic, etc.) properties in view of possible technological applications.

Acknowledgment. Financial support by the European Commission (RADSAS, NMP3-CT-2004-001561) and the Austrian Funding "Fonds zur Förderung der Wissenschaftlichen Forschung" is gratefully acknowledged. We would like to thank H. Brune for very valuable discussion.

References

(1) Barth, J. V.; Costantini, G.; Kern, K. *Nature* **2005**, *437*, 671.
(2) Rousset, S.; Repain, V.; Baudot, G.; Garreau, Y.; Lecoeur, J. *J. Phys.: Condens. Matter* **2003**, *15*, S3363. Repain, V.; Baudot, G.; Ellmer, H.; Rousset, S. *Mater. Sci. Eng.* **2002**, *96*, 178. Repain, V.; Berroir, J. M.; Rousset, S.; Lecoeur, J. *Surf. Sci.* **2000**, *447*, L152.
(3) Didiot, C.; Pons, S.; Kierren, B.; Fagot-Revurat, Y.; Malterre, D. *Nature Nanotechnology* **2007**, *2*, 617. Didiot, C.; Fagot-Revurat, Y.; Pons, S.; Kierren, B.; Malterre, D. *Surf. Sci.* **2007**, *601*, 4029. Didiot, C.; Fagot-Revurat, Y.; Pons, S.; Kierren, B.; Malterre, D.; Tejeda, A.; Rousset, S. *Appl. Surf. Sci.* **2007**, *254*, 45. Didiot, C.; Pons, S.; Kierren, B.; Fagot-Revurat, Y.; Malterre, D. *Surf. Sci.* **2006**, *600*, 3917.
(4) Xiao, W.; Ruffieux, P.; Aït-Mansour, K.; Gröning, O.; Palotas, K.; Hofer, W. A.; Gröning, P.; Fasel, R. *J. Phys. Chem. B* **2006**, *110*, 21394.
(5) Cañas-Ventura, M. E.; Xiao, W.; Wasserfallen, D.; Müllen, K.; Brune, H.; Barth, J. V.; Fasel, R. *Angew. Chem., Int. Ed.* **2007**, *46*, 1814.
(6) Brune, H.; Röder, H.; Boragno, C.; Kern, K. *Phys. Rev. B* **1994**, *49*, 2997.
(7) Stevens, J. L.; Hwang, R. Q. *Phys. Rev. Lett.* **1995**, *74*, 2078. Hwang, R. Q.; Hamilton, J. C.; Stevens, J. L.; Foiles, S. M. *Phys. Rev. Lett.* **1995**, *74*, 4242.
(8) Ling, W. L.; Hamilton, J. C.; Thürmer, K.; Thayer, G. E.; de la Figuera, J.; Hwang, R. Q.; Carter, C. B.; Bartelt, N. C.; McCarty, K. F. *Surf. Sci.* **2006**, *600*, 1735.
(9) Jacobsen, J.; Pleth Nielsen, L.; Besenbacher, F.; Stensgaard, I.; Lægsgaard, E.; Rasmussen, T.; Jacobsen, K. W.; Nørskov, J. K. *Phys. Rev. Lett.* **1995**, *75*, 489.
(10) Bendounan, A.; Cercellier, H.; Fagot-Revurat, Y.; Kierren, B.; Yu Yurov, V.; Malterre, D. *Phys. Rev. B* **2003**, *67*, 165412. Meunier, I.; Tréglia, G.; Gay, J. M.; Aufray, B.; Legrand, B. *Phys. Rev. B* **1999**, *59*, 10910.
(11) Barth, J. V.; Brune, H.; Ertl, G.; Behm, R. J. *Phys. Rev. B* **1990**, *42*, 9307.
(12) Brune, H.; Giovannini, M.; Bromann, K.; Kern, K. *Nature* **1998**, *394*, 451. Brune, H.; Bromann, K.; Röder, H.; Kern, K.; Jacobsen, J.; Stoltze, P.; Jacobsen, K.; Nørskov, J. *Phys. Rev. B* **1995**, *52*, 14380. Bromann, K.; Giovannini, M.; Brune, H.; Kern, K. *Eur. Phys. J. D* **1999**, *9*, 25.
(13) Aït-Mansour, K.; Ruffieux, P.; Xiao, W.; Gröning, P.; Fasel, R.; Gröning, O. *Phys. Rev. B* **2006**, *74*, 195418. Aït-Mansour, K.; Ruffieux, P.; Xiao, W.; Gröning, P.; Fasel, R.; Gröning, O. *J. Phys.: Conf. Ser.* **2007**, *61*, 16.
(14) Palotás, K.; Hofer, W. A. *New J. Phys.* **2007**, *9*, 393.
(15) Chambliss, D. D.; Wilson, R. J.; Chiang, S. *Phys. Rev. Lett.* **1991**, *66*, 1721. Voigtländer, B.; Meyer, G.; Amer, N. M. *Phys. Rev. B* **1991**, *44*, 10354. Meyer, J. A.; Baikie, I. D.; Kopatzki, E.; Behm, R. J. *Surf. Sci.* **1996**, *365*, L647. Tölkes, C.; Zeppenfeld, P.; Krzyzowski, M. A.; David, R.; Comsa, G. *Phys. Rev. B* **1997**, *55*, 13932.
(16) Yokoyama, T.; Yokoyama, S.; Kamikado, T.; Okuno, Y.; Mashiko, S. *Nature* **2001**, *413*, 619.
(17) Pohl, K.; Bartelt, M. C.; de la Figuera, J.; Bartelt, N. C.; Hrbek, J.; Hwang, R. Q. *Nature* **1999**, *397*, 238. Pohl, K.; de la Figuera, J.; Bartelt, M. C.; Bartelt, N. C.; Hrbek, J.; Hwang, R. Q. *Surf. Sci.* **1999**, *433*−*435*, 506. Thürmer, K.; Carter, C. B.; Bartelt, N. C.; Hwang, R. Q. *Phys. Rev. Lett.* **2004**, *92*, 106101. Thürmer, K.; Hwang, R. Q.; Bartelt, N. C. *Science* **2006**, *311*, 1272. Diaconescu, B.; Nenchev, G.; Jones, J.; Pohl, K. *Microsc. Res. Tech.* **2007**, *70*, 547.
(18) Schmid, M.; Kresse, G.; Buchsbaum, A.; Napetschnig, E.; Gritschneder, S.; Reichling, M.; Varga, P. *Phys. Rev. Lett.* **2007**, *99*, 196104; and references therein.
(19) Horcas, I.; Fernández, R.; Gómez-Rodríguez, J. M.; Colchero, J.; Gómez-Herrero, J.; Baro, A. M. *Rev. Sci. Instrum.* **2007**, *78*, 013705.
(20) Morgenstern, K.; Rosenfeld, G.; Lægsgaard, E.; Besenbacher, F.; Comsa, G. *Phys. Rev. Lett.* **1998**, *80*, 556.
(21) Zhang, L. P.; van Ek, J.; Diebold, U. *Phys. Rev. B* **1999**, *59*, 5837. Zhang, L. P.; van Ek, J.; Diebold, U. *Phys. Rev. B* **1998**, *57*, 4285.
(22) Ohtake, A.; Koguchi, N. *Appl. Phys. Lett.* **2006**, *89*, 083108.
(23) Ratsch, C.; Seitsonen, P. A.; Scheffler, M. *Phys. Rev. B* **1997**, *55*, 6750.
(24) Altman, E. I.; Colton, R. J. *Surf. Sci.* **1993**, *295*, 13.
(25) Ruffieux, P.; Palotás, K.; Gröning, O.; Wasserfallen, D.; Müllen, K.; Hofer, W. A.; Gröning, P.; Fasel, R. *J. Am. Chem. Soc.* **2007**, *129*, 5007.

NL8013378